

Regulating Anderson localization with structural defect disorder

Mouyang Cheng(程谋阳), Haoxiang Chen(陈浩翔), and Ji Chen(陈基)

Citation: Chin. Phys. B, 2024, 33 (**10**): 107201. DOI: 10.1088/1674-1056/ad711c
Journal homepage: http://cpb.iphy.ac.cn; http://iopscience.iop.org/cpb

What follows is a list of articles you may be interested in

Thermoelectric performance of XI_2 (X = Ge, Sn, Pb) bilayers

Nan Lu(陆楠) and Jie Guan(管杰)

Chin. Phys. B, 2022, 31 (**4**): 047201. DOI: 10.1088/1674-1056/ac474c

Mobility edges and reentrant localization in one-dimensional dimerized non-Hermitian quasiperiodic lattice

Xiang-Ping Jiang(蒋相平), Yi Qiao(乔艺), and Jun-Peng Cao(曹俊鹏)

Chin. Phys. B, 2021, 30 (**9**): 097202. DOI: 10.1088/1674-1056/ac11e5

Magnetotransport properties of graphene layers decorated with colloid quantum dots

Ri-Jia Zhu(朱日佳), Yu-Qing Huang(黄雨青), Jia-Yu Li(李佳玉), Ning Kang(康宁), Hong-Qi Xu(徐洪起)

Chin. Phys. B, 2019, 28 (**6**): 067201. DOI: 10.1088/1674-1056/28/6/067201

Uncertainties of clock and shift operators for an electron in one-dimensional nonuniform lattice systems

Long-Yan Gong(巩龙延), You-Gen Ding(丁友根), Yong-Qiang Deng(邓永强)

Chin. Phys. B, 2017, 26 (**11**): 117201. DOI: 10.1088/1674-1056/26/11/117201

Phase diagram of a family of one-dimensional nearest-neighbor tight-binding models with an exact mobility edge

Long-Yan Gong(巩龙延), Xiao-Xin Zhao(赵小新)

Chin. Phys. B, 2017, 26 (**7**): 077202. DOI: 10.1088/1674-1056/26/7/077202

RAPID COMMUNICATION

Regulating Anderson localization with structural defect disorder

Mouyang Cheng(程谋阳)[1], Haoxiang Chen(陈浩翔)[1], and Ji Chen(陈基)[1,2,3,4,†]

[1] *School of Physics, Peking University, Beijing* 100871, *China*
[2] *Interdisciplinary Institute of Light-Element Quantum Materials and Research Center for Light-Element Advanced Materials, Peking University, Beijing* 100871, *China*
[3] *Frontiers Science Center for Nano-Optoelectronics, Peking University, Beijing* 100871, *China*
[4] *Collaborative Innovation Center of Quantum Matter, Beijing* 100871, *China*

(Received 1 June 2024; revised manuscript received 17 August 2024; accepted manuscript online 20 August 2024)

Localization due to disorder has been one of the most intriguing theoretical concepts that evolved in condensed matter physics. Here, we expand the theory of localization by considering two types of disorders at the same time, namely, the original Anderson's disorder and the structural defect disorder, which has been suggested to be a key component in recently discovered two-dimensional amorphous materials. While increasing the degree of both disorders could induce localization of wavefunction in real space, we find that a small degree of structural defect disorder can significantly enhance the localization. As the degree of structural defect disorder increases, localized states quickly appear within the extended phase to enter a broad crossover region with mixed phases. We establish two-dimensional diagrams for the wavefunction localization and conductivity to highlight the interplay between the two types of disorders. Our theoretical model provides a comprehensive understanding of localization in two-dimensional amorphous materials and highlights the promising tunability of their transport properties.

Keywords: Anderson localization, structural defect disorder, electronic transport properties

PACS: 72.15.Rn, 73.63.–b, 61.43.–j, 61.43.Bn **DOI:** 10.1088/1674-1056/ad711c

The phenomenon that sufficient disorder results in space localization of wavefunction originates from the model of Anderson (1958).[1] A delocalized–localized transition was found at a critical order parameter value W/V, where W reflects the disorder of on-site energy, and V is the hopping integral between neighboring sites. Anderson's study inspired many theoretical works in the last century,[2] including the variable-range hopping[3,4] and the scaling theory of localization.[5–7] While analytical and numerical approaches fail to reach a consensus on the exact critical transition value of W/V, they all manage to show the same qualitative picture.[8–11] Besides, a large number of modified Anderson's models with advancing numerical calculations and scaling analyses[12–19] show the universality of wave localization in disordered systems; experiments in microwaves, acoustics, band gap materials and cold atoms all agree with the prediction[20–25] that the transport behavior exhibits a drastic change due to wavefunction localization. Disorder induced localization also plays important roles in the search for topological quantum states.[26–29] These works highlight that the localization phenomenon has a general physical picture and broad impact in various research fields.

Besides these works above with model Hamiltonian approach, there were extensive theoretical studies focused on understanding the role of defects in the transport of realistic 2D materials such as graphene.[30–34] Detailed theoretical investigations of the disorders caused by structural and topological distortions have also provided a good knowledge of the structure–property relationships in realistic amorphous materials.[35–41] In these works, localization lengths within a few nanometers were identified numerically under different scenarios, which also helped to establish a deep understanding of Anderson localization in realistic materials.[33,34]

Although the original Anderson's localization model is widely applied to interpret the delocalized–localized transition and the change of transport properties in amorphous materials, recent works have indicated that it is not always sufficient for realistic disordered materials. For example, two-dimensional (2D) amorphous monolayer carbon has been recently obtained in experiments, providing an ideal platform to examine the structure–property relationship with unprecedented precision.[42–45] In particular, Tian *et al.*[46] reported a tuning of electrical conductivity up to 9 orders of magnitude via controlling the degree-of-disorder in amorphous monolayer carbon. A variable hopping model was employed in the same work to explain the conductivity change, where a link was made between the electric conductivity and the structural disorder. The structural disorders are associated with the so-called medium range order and the structural defects, including structural holes and contaminated regions. While the physics of medium range order can boil down to the original Anderson's model, the role of the structural defects can not be

†Corresponding author. E-mail: ji.chen@pku.edu.cn

© 2024 Chinese Physical Society and IOP Publishing Ltd

captured by the original model and the existing extensions. In addition to monolayer carbon, structural defects can also be created in a large number of 2D materials using different experimental techniques, providing opportunity to engineer their properties with structural defect disorders.[40,47–49]

In this work, we propose a new extension of the Anderson localization model by considering simultaneously two different mechanisms of disorders on the 2D lattice. Two order parameters are introduced, one corresponds to the original Anderson's disorder (W/V) and the other characterizes the structural defect disorder. We then perform systematic numerical calculations and analyses, which show that both disorders can induce wavefunction localization, and the interplay between the two distinct types of disorders gives rise to non-trivial localization behavior. A diagram of localization is given, where the cooperation and competition of the two localization mechanisms are fully revealed. The electrical conductivity is calculated based on the Kubo–Greenwood formula,[50,51] which further illustrates that both types of disorders have significant impacts on the electron transport.

We start from the non-interacting tight-binding Hamiltonian on a 2D square lattice with a single electron band

$$\hat{H} = \sum_{j,k}\left(V_{x,jk}\hat{a}^{\dagger}_{j+1,k}\hat{a}_{j,k} + V_{y,jk}\hat{a}^{\dagger}_{j,k+1}\hat{a}_{j,k}\right) + \text{h.c.} + \sum_{j,k} E_{jk}\hat{a}^{\dagger}_{j,k}\hat{a}_{j,k},$$

where $V_{x,jk}$ and $V_{y,jk}$ stand for the hopping energy from site (j,k), E_{jk} is the potential energy of site (j,k). $\hat{a}^{\dagger}_{j,k}$ and $\hat{a}_{j,k}$ are one electron creation and annihilation operators at site (j,k). A discussion about the relation between our model and real material is detailed in the supplementary information (SI) Section I (SI.I). Diagonalization of the corresponding hopping matrix results in the Hamiltonian's eigenstates. In the Anderson localization model, disorder is described by a random distribution of the on-site energy within $[\varepsilon - W/2, \varepsilon + W/2]$. When neglecting the off-diagonal disorder, namely, choosing a constant hopping term V, a dimensionless order parameter (W/V) is used to characterize the degree of disorder.

Inspired by the structural defects in 2D amorphous materials, such as atomic holes and contaminated regions, we introduce a new parameter to describe the disorder, namely, the ratio of forbidden sites for electrons (λ). To model this new disorder, we randomly choose some of the sites on the square lattice, and set their on-site potential as E_{m}, which is significantly larger than the magnitude of the on-site energy and the hopping kinetic energy. The effect is obvious that the extremely large on-site potential creates a huge eigenvalue, making the corresponding site physically forbidden for electronic occupation. Thus, the direct outcome is that these high energy sites are forbidden for electron hopping, which may also contribute to the localization of wavefunction.

Figure 1 shows a map of the on-site energy on a 30×30 square lattice, illustrating the coexistence of the two types of disorders. The red patches correspond to the forbidden sites and the on-site energy fluctuation due to Anderson disorder is shown with blue colors. We expect both types of disorders to make contribution to the localization of wavefunction and reduce the electrical conductivity. In the following, we discuss numerical results performed on a 30×30 square lattice, where W/V varies from 0 to 8 and λ is within 0.25.[52] The Fermi energy is set as $E_{\text{F}} = 0$ and the energy of forbidden sites is set as $E_{\text{m}} = 1000$ V. Configuration averages are taken over $n_{\text{paths}} = 200$ randomly generated models to get converged results. More details, convergence tests, additional results and extended analyses are discussed in the SI.

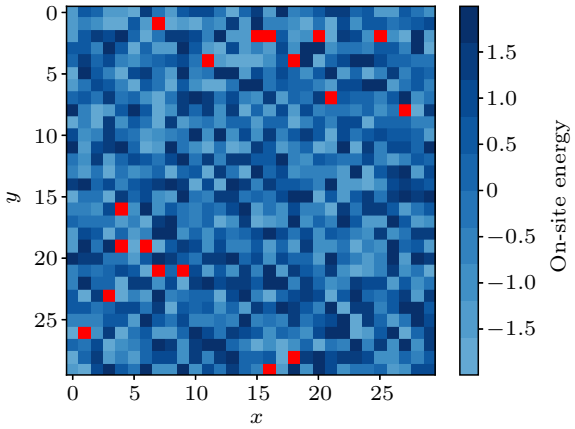


Fig. 1. A potential energy map on a 30×30 square lattice with two types of disorders. The two order parameters are $W/V = 4$ and $\lambda = 0.02$. The red isolated patches indicate random distributed forbidden sites with $E_{\text{m}} = 1000$. The blue colored patches correspond to the disorder from random distribution of the on-site energy.

To have a direct view of how wavefunction localizes, we calculate the occupation number $|\psi_i|^2$ for each site i. Figure 2(a) shows an example of the extended state, where many sites have non-zero occupations. For a localized state, the electron only occupies one site as displayed in Fig. 2(b). A larger set of visualization diagrams are presented in SI.II. In Figs. 2(c) and 2(d) we show the wavefunctions of three states in the extended system and the localized system along one lattice dimension, respectively. For an extended system, wavefunctions of many states are delocalized as in Fig. 2(c), while for a localized system every state has its electron occupying one site. In addition to the extended phase and the localized phase, we also identify the existence of a broad transition regime where mixed phases may appear.

To quantify the localization behavior, we calculate the normalized participation ratio (NPR),[53,54] which is defined as

$$\text{NPR}_i = \left(L^2 \sum_{n=1}^{N^2} |\phi_i^n|^4\right)^{-1},$$

where N^2 sites are considered, $L = Na$ is size of the system, a is the lattice constant and ϕ_i^n is the component of the i-th eigenfunction projected on the n-th site.

For 2D systems, NPR should satisfy the following conditions:

$$\mathrm{NPR} \sim \begin{cases} \xi^{-2}, & \text{for extended states,} \\ L^{-2}, & \text{for localized states,} \end{cases}$$

where ξ is a constant characterizing the localization length of the corresponding state. Therefore, for large L, NPR remains finite for extended states and vanishes for localized states.

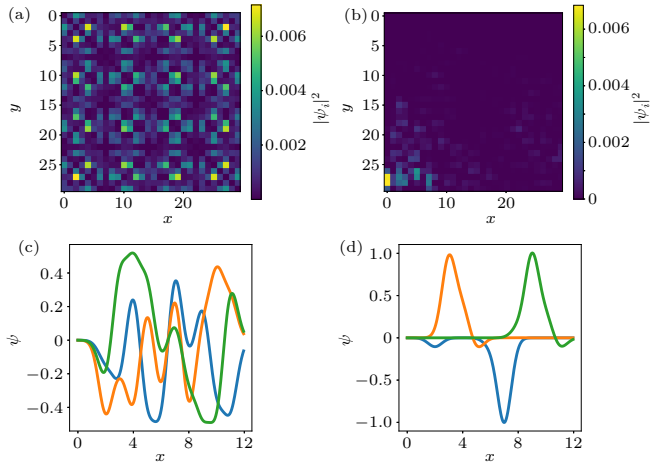


Fig. 2. Visualization of the extended and localized states. [(a) and (b)] Occupation number of a randomly selected state on the two-dimensional lattice from an extended system ($W/V = 0$; $\lambda = 0$) and a localized system ($W/V = 0$; $\lambda = 0.2$). [(c) and (d)] Three wavefunctions plotted along one lattice dimension. The wavefunctions are real due to the Hermitian matrix.

Figures 3(a) and 3(b) plot NPR values of all eigenstates under $\lambda = 0$–0.5, $W/V = 0$ and $W/V = 0$–8, $\lambda = 0$, respectively. Each NPR curve represents one set of parameters. According to our design of the Hamiltonian, as λ increases only λN^2 sites should have vanishing NPR, and one expects a discontinuous function of the NPR curve plotted as a function of the state index. However, figure 3(a) shows that the curves drop to zero continuously apart from the fully extended system (blue line). The overall non-vanishing NPR of the other states also decays to zero as λ increases. At around $\lambda = 0.4$, the whole NPR curve is reduced to $\sim L^{-2}$, where a full localization of the whole system occurs. These observations show that (i) the structural defect disorder can induce a mixture of localized and extended states in the system; (ii) a small portion of structural defects can cause global localization of the whole system. In contrast, the original Anderson type disorder W/V induces a smoother transition from the extended phase at $W/V = 0$ to around $W/V = 6$ where most of the states have vanishing NPR.

If we take these two order parameters together into consideration, the system consists of a rich variety of phases. To further classify them, we define a new parameter $\eta = \frac{\langle \mathrm{NPR} \rangle(N/2)}{4\langle \mathrm{NPR} \rangle(N)}$, where $\langle \mathrm{NPR} \rangle(N)$ is the average value of all eigenstates' NPR for an $N \times N$ lattice. The definition of η is inspired by the fact that for the fully localized phase NPR $\sim N^{-2}$, while for the extended phase NPR of all eigenstates is independent of N. With such a definition, we have $\eta = 0.25$ for pure extended states, and $\eta = 1$ for pure localized states. Figure 3(c) shows a colored contour diagram of η as a function of the two order parameters W/V and λ.

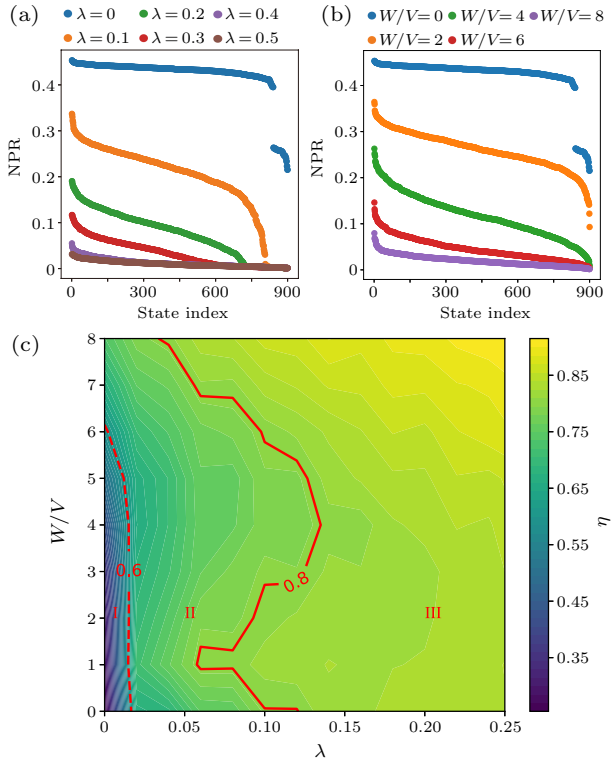


Fig. 3. Quantification of localization under different order parameters. (a) and (b) NPR values plotted for different eigenstates under different order parameters. Finite and vanishing NPRs correspond to the extended and localized states, respectively. (a) NPR for $W/V = 0$ and $\lambda = 0, 0.1, 0.2, 0.3, 0.4, 0.5$ (lines from top to bottom). (b) NPR for $\lambda = 0$ and $W/V = 0, 2, 4, 6, 8$ (lines from top to bottom). (c) The localization contour diagram plotting η as a function of the order parameters W/V and λ. The red lines indicate the two boundaries ($\eta = 0.6$ and $\eta = 0.8$) separating three phase regimes: (I) the extended phase, (II) the crossover regime with mixed phases and (III) the localized phase.

We classify the extended, crossover and localized phases revealed above as I, II and III, respectively. As a result, there are two steps in the localization transition, namely, the step from the extended phase to the crossover regime with mixed phases; and the step to the fully localized phase. To this end, we choose two critical values for η, which are indicated as red lines in Fig. 3. For the boundary between the extended phase and the crossover regime, we recall that the original Anderson transition point is near $W/V \approx 6$[55] and $\lambda = 0$, so we take the contour line of η which crosses this conventional transition point, i.e., $\eta_1 = 0.6$, to represent the boundary. The second boundary is set at $\eta_2 = 0.8$ because numerical calculations show that as λ rises, η drastically increases to $\eta = 0.75$–0.85 and then slowly approaches $\eta = 0.9$–1 for larger disorder

(SI.III). We note that in real systems η may not reach the ideal value 1 because of finite N and incompleteness of localization. Therefore, $\eta_2 = 0.8$ can be considered as the boundary entering the fully localized phase.

It is quite clear that the three phase regions are well separated by the variation of λ. Tuning the ratio of randomly distributed forbidden sites within a range of approximately 10% can already achieve the transition from the extended phase to the fully localized phase. This is not affected significantly by the choice of the other parameter W/V given that the value is within a reasonable range. This observation is in good agreement with previous studies concerning various sources of structural defects.[33,34] In the SI.IX we show results calculated on a honeycomb lattice, where the same conclusion can be reached.

An even more interesting observation is that the two types of disorders are not only trivially additive to each other, but cooperation and competition might exist. With a finite λ, contour lines of η extend towards the left as W/V increases from 0 to 1, then rightwards until W/V increases to 4. The change of the direction of contour lines means that the localization firstly increases and is then suppressed before $W/V = 4$. The reason for such an anomaly is further discussed in SI.V. It is also worth noting that a similar re-entrant behavior was recently revealed in the one-dimensional model of quasi-periodic lattice with staggered on-site potential.[56] The key point is that while both Anderson disorder and hole defect disorder can induce significant localization separately, their combination renders a more complicated picture than one might anticipate.

To further understand how the two types of disorders affect the transport property, we calculate the conductivity σ using the Kubo–Greenwood formula[50,51]

$$\sigma = \lim_{\omega\to 0}\left(\pi/(\omega L^2)\right)\int \mathrm{d}E' \sum_{\alpha,\beta}\sum_{j}|\langle\alpha|J_x(j)|\beta\rangle|^2 \times\delta\left(E'+\omega-E_\beta\right)\delta\left(E'-E_\alpha\right),$$

where L is the length of the system, $|\alpha\rangle$, $|\beta\rangle$ are eigenstates of the Hamiltonian and correspond to eigenvalues $E_\alpha < E < E_\beta$. For a current flows in the x-direction, $J_x(j)$ is the current operator, and is defined as

$$J_x(j) = \mathrm{i}e\sum_k V_{x,jk}\left({a_{j,k}}^\dagger a_{j-1,k} - \mathrm{h.c.}\right).$$

More computational details are discussed in SI.VI, and calculations for larger lattice size N using linear scaling methods[57–59] are supplemented in SI.XI.

Figure 4 plots the conductivity for different parameters of W/V and λ. The two critical contour lines with values η_1 and η_2 separating regions of different degrees of localization are also shown. Although it is expected that the increase of both disorders can lead to the reduction of conductivity, it is interesting to see that the effects of disorder on the conductivity do not follow exactly the same trend as the localization. It suggests that different from the conventional Anderson localization, a metal–insulator transition is no longer necessarily synchronized with the extended–localized transition. Only a small portion of the forbidden sites are needed to cause the localization, but to induce a reduction of the conductivity a quite large number of forbidden sites are needed. This is reasonable because localized electrons can still contribute to conductivity via hopping mechanisms, and only when all the hopping paths are blocked by enough number of forbidden sites, the conductivity can be strongly suppressed. From the perspective of the density of states (DOS) as displayed in SI.VIII, DOS near the Fermi energy decreases more rapidly as a function of W/V compared to that of λ.

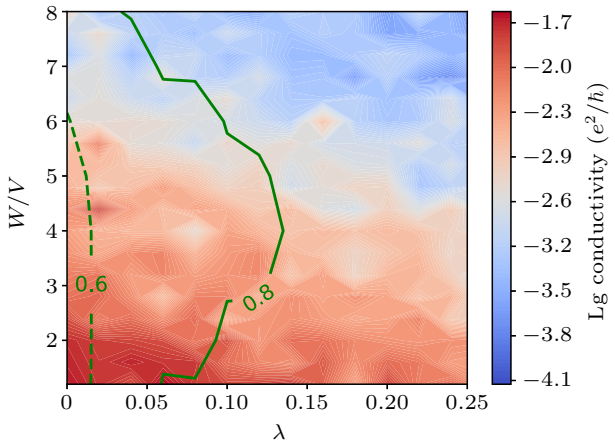


Fig. 4. Conductivity diagram as a function of the order parameters W/V and λ. For better visualization, the $W/V < 1.2$ part is not shown because the decay near $W \sim 0+$ is too rapid. Green lines show the two localization boundaries from Fig. 3 ($\eta_{1,2} = 0.6, 0.8$).

It is worth noting that in the studies of Tian *et al.* the insulating samples have many structural holes and contaminated sites,[46] corresponding to $\lambda > 0.5$ and $W/V < 3$ (SI.X). In that regime a variable range hopping model is more suitable and can describe the conductivity behavior very well. In the SI.IX we also show numerical results and analyses on the honeycomb lattice, which resembles the true structure of amorphous monolayer carbon. The enhancement of localization due to structural defect disorder is also observed, supporting the main conclusion of this study. However, we shall note that the honeycomb lattice involves a new degree of complexity due to the semi-metallic nature. One can notice the anomalous behavior in the weak localization regime and other differences in other parameter regimes. While some behaviors can be straightforwardly understood by the semi-metallic band structure,[60,61] further theoretical works are desired to reveal more details about the impact of structural defect disorder.[62,63]

In the future, when the quality of 2D amorphous materials is improved to a regime where the number of forbidden sites is within 20%, we expect the conductivity to follow the current

model. Even in this regime, one can achieve a tuning of the conductivity by as much as 2 orders of magnitude. In contrast, when λ is small, the Anderson disorder can suppress the conductivity more effectively, where the conductivity reduces by at most 7 magnitudes when W/V increases beyond 6. A similar behavior of both disorders is that the decay of conductivity mainly occurs at weak localization, namely, small W/V and λ (SI.VII).

While the electrical conductivity reveals rich information of transport properties, it is more rigorous to extract the transport localization length ξ to the thermodynamic limit when analyzing localization effects. Therefore, we further carry out a scaling analysis of the dc conductivity discussed above. Within the strong localization regime, the electrical conductance decays exponentially with the system size N. i.e.,

$$\sigma(N) \propto \mathrm{e}^{-N/\xi}.$$

In the weak localization regime, the exponential relation does not hold, so by extracting ξ as a function of W/V and λ, we are able to identify the transition line for localization of transport properties at $1/\xi \to 0$. The weak and strong localization regimes are divided in Fig. 5, where we take a linear extrapolation from finite $1/N$ to $1/N = 0$. Similar to the wave function localization diagram in Fig. 3, there is a reentrant localization behavior for W/V within 2 and 4, indicated by the dark red band. Comparison between the wave function localization diagram, the conductivity diagram and the transport localization length diagram demonstrates consistently that the interplay of the two types of disorders creates a much more complicated picture of localization.

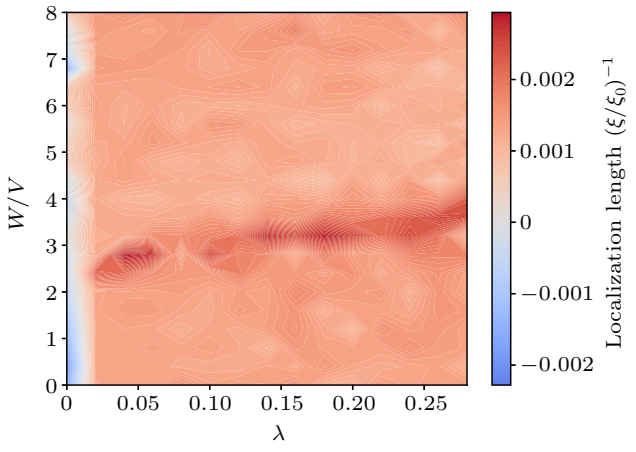


Fig. 5. Transport localization length ξ as a function of the order parameters W/V and λ. $1/\xi = 0$ marks the division line between the weak localization regime (blue part) and the strong localization regime (red part).

To conclude, in this work we introduce an extension of the Anderson's localization model with randomly distributed forbidden sites, inspired by the structural defect disorder in 2D amorphous materials such as structural holes and contaminating sites. Numerical calculations and analyses show that the structural defect disorder can interplay with Anderson's disorder to enhance the localization, driving the extended phase first to a mixed phase then to a fully localized phase, providing a more versatile control of the electrical conductivity of 2D materials. Our model provides a more comprehensive understanding of the localization phenomenon and electronic transport in 2D systems, which shall motivate further investigations, for example, the role of the interplay of different types of disorders on other transport properties,[64] on other emergent phenomena,[29,65–67] and in three-dimensional disordered systems.[68,69]

Acknowledgments

The authors thank Huifeng Tian and Lei Liu for providing original experimental data and helpful discussions. We also thank Huaqing Huang for helpful discussions. Project supported by the National Natural Science Foundation of China (Grant No. 92165101), the National Key R&D Program of China (Grant No. 2021YFA1400500), the Strategic Priority Research Program of Chinese Academy of Sciences (Grant No. XDB33000000), and the Beijing Natural Science Foundation (Grant No. JQ22001). We are grateful for computational resources supported by High-performance Computing Platform of Peking University.

References

[1] Anderson P W 1958 *Phys. Rev.* **109** 1492
[2] Lee P A and Ramakrishnan T V 1985 *Rev. Mod. Phys.* **57** 287
[3] Mott N F 1968 *Rev. Mod. Phys.* **40** 677
[4] Mott N F 1968 *Philosophical Magazine* **17** 1259
[5] Anderson P W, Thouless D J, Abrahams E and Fisher D S 1980 *Phys. Rev. B* **22** 3519
[6] Abrahams E, Anderson P W, Licciardello D C and Ramakrishnan T V 1979 *Phys. Rev. Lett.* **42** 673
[7] Lee P A and Fisher D S 1981 *Phys. Rev. Lett.* **47** 882
[8] Edwards J T and Thouless D J 1972 *J. Phys. C: Solid State Phys.* **5** 807
[9] Stein J and Krey U 1980 *Zeitschrift fur Physik B* **37** 13
[10] Thouless D 1974 *Physics Reports* **13** 93
[11] Abou-Chacra R, Thouless D J and Anderson P W 1973 *J. Phys. C: Solid State Phys.* **6** 1734
[12] Piao X and Park N 2022 *ACS Photonics* **9** 1655
[13] Corona-Patricio G, Kuhl U, Mortessagne F, Vignolo P and Tessieri L 2019 *New J. Phys.* **21** 073041
[14] Sutradhar J, Mukerjee S, Pandit R and Banerjee S 2019 *Phys. Rev. B* **99** 224204
[15] Agarwal K, Ganeshan S and Bhatt R N 2017 *Phys. Rev. B* **96** 014201
[16] Todorov T 2002 *J. Phys.: Condens. Matter* **14** 3049
[17] Furusaki A 1999 *Phys. Rev. Lett.* **82** 604
[18] Sugiyama T and Nagaosa N 1993 *Phys. Rev. Lett.* **70** 1980
[19] Hetényi B, Parlak S and Yahyavi M 2021 *Phys. Rev. B* **104** 214207
[20] Chabanov A A, Stoytchev M and Genack A Z 2000 *Nature* **404** 850
[21] Weaver R 1990 *Wave Motion* **12** 129
[22] Hu H, Strybulevych A, Page J H, Skipetrov S E and van Tiggelen B A 2008 *Nat. Phys.* **4** 945
[23] Schwartz T, Bartal G, Fishman S and Segev M 2007 *Nature* **446** 52
[24] Chabé J, Lemarié G, Grémaud B, Delande D, Szriftgiser P and Garreau J C 2008 *Phys. Rev. Lett.* **101** 255702
[25] Lagendijk A, van Tiggelen B and Wiersma D S 2009 *Physics Today* **62** 24
[26] Li J, Chu R L, Jain J K and Shen S Q 2009 *Phys. Rev. Lett.* **102** 136806
[27] Groth C W, Wimmer M, Akhmerov A R, Tworzydło J and Beenakker C W J 2009 *Phys. Rev. Lett.* **103** 196805

[28] Song J, Liu H, Jiang H, Sun Q F and Xie X C 2012 *Phys. Rev. B* **85** 195125
[29] Ivaki M N, Sahlberg I and Ojanen T 2020 *Phys. Rev. Research* **2** 043301
[30] Lherbier A, Blase X, Niquet Y M, Triozon F and Roche S 2008 *Phys. Rev. Lett.* **101** 036808
[31] Lherbier A, Biel B, Niquet Y M and Roche S 2008 *Phys. Rev. Lett.* **100** 036803
[32] Leconte N, Moser J, Ordejón P, Tao H, Lherbier A, Bachtold A, Alsina F, Torres C M S, Charlier J C and Roche S 2010 *ACS Nano* **4** 4033
[33] Lherbier A, Dubois S M M, Declerck X, Roche S, Niquet Y M and Charlier J C 2011 *Phys. Rev. Lett.* **106** 046803
[34] Lherbier A, Dubois S M M, Declerck X, Niquet Y M, Roche S and Charlier J C 2012 *Phys. Rev. B* **86** 075402
[35] Cresti A, Nemec N, Biel B, Niebler G, Triozon F, Cuniberti G and Roche S 2008 *Nano Research* **1** 361
[36] Kapko V, Drabold D A and Thorpe M F 2010 *Physica Status Solidi (b)* **247** 1197
[37] Van Tuan D, Kumar A, Roche S, Ortmann F, Thorpe M F and Ordejon P 2012 *Phys. Rev. B* **86** 121408
[38] Foa Torres L E F, Roche S and Charlier J C 2020 *Introduction to Graphene-Based Nanomaterials: From Electronic Structure to Quantum Transport*, 2nd Edn. (Cambridge University Press)
[39] Thapa R, Ugwumadu C, Nepal K, Trembly J and Drabold D 2022 *Phys. Rev. Lett.* **128** 236402
[40] Zhang Y T, Wang Y P, Zhang X, Zhang Y Y, Du S and Pantelides S T 2022 *Nano Lett.* **22** 8018
[41] Antidormi A, Colombo L and Roche S 2022 *Nano Materials Science* **4** 10
[42] Kotakoski J, Krasheninnikov A V, Kaiser U and Meyer J C 2011 *Phys. Rev. Lett.* **106** 105505
[43] Eder F R, Kotakoski J, Kaiser U and Meyer J C 2014 *Scientific Reports* **4** 4060
[44] Joo W J, Lee J H, Jang Y, Kang S G, Kwon Y N, Chung J, Lee S, Kim C, Kim T H, Yang C W, *et al.* 2017 *Science Advances* **3** e1601821
[45] Toh C T, Zhang H, Lin J, Mayorov A S, Wang Y P, Orofeo C M, Ferry D B, Andersen H, Kakenov N, Guo Z, Abidi I H, Sims H, Suenaga K, Pantelides S T and Özyilmaz B 2020 *Nature* **577** 199
[46] Tian H, Ma Y, Li Z, Cheng M, Ning S, *et al.* 2023 *Nature* **615** 56
[47] Zhao H, Chen X, Wang G, Qiu Y and Guo L 2019 *2D Materials* **6** 032002
[48] Hong S, Lee C S, Lee M H, Lee Y, Ma K Y, Kim G, Yoon S I, Ihm K, Kim K J, Shin T J, *et al.* 2020 *Nature* **582** 511
[49] Shin D, Wang G, Han M, Lin Z, O'Hara A, Chen F, Lin J and Pantelides S T 2021 *Phys. Rev. Materials* **5** 044002
[50] Kubo R 1957 *J. Phys. Soc. Jpn.* **12** 570
[51] Greenwood D A 1958 *Proceedings of the Physical Society* **71** 585
[52] Our model has a constraint that $\lambda < 0.5$. This is because as $\lambda > 0.5$, the wavefunction starts to delocalize as λ continues to rise. This can be easily shown at $\lambda = 1$, where the Hamiltonian is simply $\hat{H}(\lambda = 1) = E_{\mathrm{m}}\hat{I} + \hat{H}(\lambda = 0)$ resulting in the same eigenstates as $\hat{H}(\lambda = 0)$, which returns to the $\lambda = 0$ case.
[53] Li X and Sarma S D 2020 *Phys. Rev. B* **101** 064203
[54] Roy S, Mishra T, Tanatar B and Basu S 2021 *Phys. Rev. Lett.* **126** 106803
[55] Mott N F and Davis E A 2012 *Electronic processes in non-crystalline materials* (Oxford University Press)
[56] Padhan A, Giri M K, Mondal S and Mishra T 2022 *Phys. Rev. B* **105** L220201
[57] García J H, Covaci L and Rappoport T G 2015 *Phys. Rev. Lett.* **114** 116602
[58] Ködderitzsch D, Chadova K and Ebert H 2015 *Phys. Rev. B* **92** 184415
[59] Groth C W, Wimmer M, Akhmerov A R and Waintal X 2014 *New J. Phys.* **16** 063065
[60] Carva K, Sanyal B, Fransson J and Eriksson O 2010 *Phys. Rev. B* **81** 245405
[61] Holmström E, Fransson J, Eriksson O, Lizárraga R, Sanyal B, Bhandary S and Katsnelson M I 2011 *Phys. Rev. B* **84** 205414
[62] Khveshchenko D V 2006 *Phys. Rev. Lett.* **97** 036802
[63] Onoda M, Avishai Y and Nagaosa N 2007 *Phys. Rev. Lett.* **98** 076802
[64] Zhang Y T, Wang Y P, Zhang Y Y, Du S and Pantelides S T 2022 *Appl. Phys. Lett.* **120** 222201
[65] Jiang H, Wang L, Sun Q F and Xie X C 2009 *Phys. Rev. B* **80** 165316
[66] Agarwala A and Shenoy V B 2017 *Phys. Rev. Lett.* **118** 236402
[67] Wang C, Cheng T, Liu Z, Liu F and Huang H 2022 *Phys. Rev. Lett.* **128** 056401
[68] Guo H M, Rosenberg G, Refael G and Franz M 2010 *Phys. Rev. Lett.* **105** 216601
[69] Ying T, Gu Y, Chen X, Wang X, Jin S, Zhao L, Zhang W and Chen X 2016 *Science Advances* **2** e1501283